Title

ANODIC BEHAVIOR OF COPPER IN AQUEOUS SOLUTIONS DETERMINED WITH A SELF-NULLING AUTOMATIC ELLIPSOMETER

Authors

Mathieu, H.J.
Muller, R.H.

Publication Date

1973-12-01

ANODIC BEHAVIOR OF COPPER IN AQUEOUS SOLUTIONS DETERMINED WITH A SELF-NULLING AUTOMATIC ELLIPSOMETER

H. J. Mathieu and R. H. Muller

December 1973

Prepared for the U.S. Atomic Energy Commission
under Contract W-7405-ENG-48

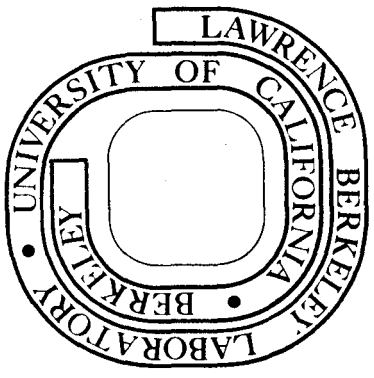

DISCLAIMER

ANODIC BEHAVIOR OF COPPER IN AQUEOUS SOLUTIONS DETERMINED WITH A SELF-NULLING AUTOMATIC ELLIPSOMETER

H. J. Mathieu and R. H. Muller

Inorganic Materials Research Division, Lawrence Berkeley Laboratory and

Department of Chemical Engineering; University of California

Berkeley, California 94720

ABSTRACT

An investigation of the growth of anodic films on copper under free and forced convection conditions was carried out with an automatic ellipsometer. These <u>in situ</u> measurements in an aqueous $NaClO_3$ solution show for current densities of 0.08-1.2 A/cm^2 the presence of a porous Cu_2O layer. The porosity is affected by current density and flow velocity. A mass transfer boundary layer of dissolved $Cu(ClO_3)_x$ (x = 1,2) has also been observed.

INTRODUCTION

Previous investigations[1-4] showed the complexity of the anodic film growth on copper under free and forced convection. As a first application of the newly built ellipsometer,[5] capable to follow anodic film growth in situ, it appeared desirable to investigate the character of film growth of Cu_xO (x = 1-2) in aqueous solutions. This automatic ellipsometer can follow a Cu_2O film growth of about 10 Å/ms[6] for 0 to 500Å thickness. Experimental growth rates observed throughout the course of this investigation were in the order of 300 Å/s. A schematic arrangement of the ellipsometer is shown in Fig. 1. This self-nulling ellipsometer is based on the application of the Faraday effect, using two Faraday magnets to rotate electronically the plane of polarization of analyzer and polarizer. The current passed through these two magnets is monitored and calibrated in degrees of rotation. From these two measured quantities the ellipsometric parameter ψ and Δ can be derived.[7] They are related to the refractive index of a substrate and film(s) covering the substrate. Various computer programs were used to perform this conversion.[8,9] Optical constants for copper (n = 0.93-2.39 i,[19] n = 1.1-2.54i present, n = 0.72-2.42 i[20]) and the copper oxides are available (Cu_2O: n = 2.75-0.195 i,[14] n = 2.75-0.27 i present, 3-0.19 i to 2.5-0.265 i,[21] CuO: n = 2.57-0.539 i[15]). All experiments were carried out at one wavelength λ = 546.1 nm.

EXPERIMENTS

Experiments were carried out at room temperature in an open cell with stagnant solution and a flow channel cell. Cross sections of both are shown in Figs. 2 and 3.[10] Anode and cathode of the open cell were separated by a cloth diaphragm to keep the anode free of hydrogen produced at the cathode. The material used for the cathode was stainless steel. The same anodes could be used in open cell and flow channel and were easily exchanged from the back of both cells. The alignment of the anode with respect to the ellipsometer was carried out by using leveling screws after the anode had been inserted into the cell. The 1.2×3 cm copper electrodes (purity 99.9%), cast in epoxy, were ground and polished with 1μ diamond abrasives using usual procedures, then cathodically cleaned in 1 m NaOH solution for 3 min at 100 mA/cm^2. 2M $NaClO_3$ solution (pH = 5.5) was used for all anodic film growth experiments described here. This solution was chosen because of its previous use[1,2,4] and because no oxygen is evolved at the anode during the experiments. The refractive index of the electrolyte was determined with a refractometer to be n = 1.3524 at room temperature. The power supply could be used in a galvanostatic or potentiostatic mode.

Figure 4 shows a typical recorder-chart (solid curves) of the change of the ellipsometer parameters ψ and Δ during anodic polarization of a copper electrode under free convection conditions at 123 mA/cm^2. Galvanostatic and potentiostatic experiments showed no significant difference. Also the anode potential before and after film growth was measured vs a Calmoel reference electrode. At pH = 5.5 the potentials were below

100 mV (SHE) before film growth and 265 mV (SHE) after an anodic film had been formed. The latter potential established itself within 20 mV after 5 sec following interruption of current. The potential became steady after about 4 min. It can be seen in Fig. 4 that both ellipsometer parameters do not change much during the first 5.5 sec. But after this induction period a fast change takes place, resulting in a curve, which is similar to a damped oscillation. Increasing the current density up to 550 mA/cm^2 showed (Fig. 6) a decrease of oscillation amplitudes. The copper electrodes were removed from the cell after each experiment and inspected visually. For low current densities (80-125 mA/cm^2) the copper electrode was covered with a shiny well-adhering solid brown layer. At higher current densities (125-550 mA/cm^2) it was observed, that the oxide films became more porous, were thicker, less dense and less adhering. Above 550 mA/cm^2 (to 1200) a layer of about 3000 Å (approximately 50% porosity) lifted off from the copper electrode similar to previous observations,[1,4] however, no electrical oscillations were observed. The remaining surface was pitted and its roughness not suitable for an ellipsometric measurement (worse than previous experience with 40μ roughness). In addition, the time for the induction period changed, which is shown in Table I.

Experiments with a flow velocity (u>0 cm/s) showed a similar effect on ψ and Δ with increased damping at increased flow rates. It was observed that at a flow velocity of u = 65 cm/s, hardly any oscillation was visible anymore. The induction period increased by increasing flow velocities at constant current density. Figure 7 shows four curves experimentally obtained at various flow velocities at 125 mA/cm^2. For

high velocities u > 14 cm/s no lift-off of any oxide layer, even for current densities up to 1.2 A/cm^2, was observed.

DISCUSSION

The behavior of Ψ and Δ during the induction period is given in Fig. 4. In order to explain this dependence, one has to assume a very thin film of Cu_2O oxide of about 6Å already present on the metal surface at the beginning of the anodic polarization. This film appears to be due to oxidation during the filling and alignment process of the cell. Measurements taken in the open and flow channel cells show that even without any current passing the anode, an oxide film grows slowly up to a thickness of about 20Å (Fig. 8). The presence of cuprous oxide was confirmed by measuring the electrochemical potential between the copper electrode and a calomel reference electrode.[11] The thickness of the thin oxide layer covering the copper surface at the beginning of each experiment varied slightly between 6-20Å, depending on the time between inserting the electorde into the cell and the beginning of the anodic current flow. If one further assumes a growth of a mass transfer layer of a solution of $Cu(ClO_3)_x$ (x = 1.2) from 0 to about 150μ one can explain the experimentally obtained ellipsometer data during the induction period with the help of this dual layer model (Fig. 4, 9, 10).[12] The results are not very sensitive to the thickness assumed for the mass transfer boundary layer. The value of 150μ chosen seems resonable. After the formation of a boundary layer an oxide film begins to grow. For current densities up to 125 mA/cm^2 the experimental curve, shown in Fig. 4, can be explained if one assumes a compact oxide layer forming on the copper with a mass transfer boundary layer of constant thickness (150μ) being present on top of it. The refractive index of Cu_2O was assumed to be $n = 2.75-0.25i$ at

λ = 546.1 nm.[14] After about 15s the experimental curve shows a deviation from computed valves based on solid Cu_2O (Fig. 5). This deviation can be accounted for if one assumes that a porous oxide layer, begins to grow, after a compact layer of Cu_2O of about 2500Å has formed (this case can at present not be separated from a transformation of the compact into a porous layer). The porosity of the oxide layer has been assumed to result in a decrease of the real part of the refractive index. The dashed curve in Fig. 4 assumes the formation of a porous layer of refractive index of n = 2.05-0.25i at λ = 546.1 nm corresponding to a porosity of about 25%.[13]

Comparison of the computed curves in Fig. 4 with those in Fig. 5, derived previously for a compact cuprous oxide film, illustrates the improved agreement with measurements due to the consideration of the initial oxide present, the build-up of the mass-transfer boundary layer and the conversion of a compact to a porous oxide film.

Figure 11 shows the Ψ vs Δ plot for varying the real part of the refractive index from 2.75 to 1.40 with a constant imaginary part of 0.25, and assuming a constant boundary layer of n = $1.352-10^{-4}$i and 150μ thickness above the oxide. Comparing Fig. 11 with Fig. 7 one sees the influence of decreasing the real part of the refractive index (corresponding to an increase in porosity). All experimental data can be explained using this film layer model of a compact layer of cuprous oxide on copper covered with a porous oxide film, the porosity of which changes with increasing current density and increases flow velocity.

The formation of a CuO can be excluded by the following argument. First, looking at Fig. 11, one sees that a CuO layer of refractive index $n = 2.57-0.539i$ at $\lambda = 546.1$ nm[15] has a similar effect as a porous Cu_2O film with refractive index of $n = 2.05-0.25i$. But looking at Figs. 11 and 7, one sees that at the beginning of the film growth experiments the observed curves a, b and c follow the curves computed for an assumed porosity, whereas a CuO film would deviate from this behavior. Second, a change in valence from $x = 1$ to $x = 2$ in Cu_xO would mean that the experimental ψ vs Δ plots would asymptotically approach the properties of bulk CuO, indicated by the end-point of curve f in Fig. 11. But the experimentally obtained plots go beyond the CuO behavior and follow more closely the curves with assumed increased porosity. Third, the electrochemical potentials between anode and reference electrode show the presence of Cu before and Cu_2O after film growth according to the potentials expected[11] for these materials. Optical computations for inhomogeneous films with gradually increasing porosity toward the solution-side, showed behavior not in agreement with observations. Therefore, it can be concluded that under free as well as under forced convection conditions porous layers of Cu_2O are formed.

ACKNOWLEDGEMENTS

This work was conducted under the auspices of the U. S. Atomic Energy Commission. The first author was supported by Deutsche Forschungsgemeinschaft. Mr. W. T. Giba has built both electrolytic cells and prepared Figs. 2 and 3.

Table I. Induction period τ for the onset of anodic oxide formation on Cu in stagnant solution of 2M $NaClO_3$

$i \frac{A}{cm^2}$	τ(s)	$i\sqrt{\tau}$
0.082	3.5	0.15
0.112	5	0.25
0.210	5.8	0.51
0.38	2.8	0.64
0.43	2.1	0.62
0.502	1.6	0.63
1.2	0.25	0.6

REFERENCES AND REMARKS

1. J. F. Cooper, R. H. Muller and C. W. Tobias, UCRL-19618 (1970).
2. K. Kinoshita, Studies on the Anodic Dissolution of Copper at High Current Densities (Ph. D. Thesis), UCRL-19051, August, 1969.
3. D. Landolt, R. H. Muller and C. W. Tobias, J. Electrochem. Soc. 116, 1384 (1969).
4. K. G. Hellyar, Cinematic Studies of the Anodic Dissolution of Metals at High Current Densities (M. S. Thesis), LBL-157, September, 1971.
5. H. J. Mathieu, D. E. McClure and R. H. Muller, submitted to Rev. Sci. Instr., LBL-2256, 1973.
6. H. J. Mathieu, and R. H. Muller, submitted to Appl. Optics, LBL-1857 (1973).
7. R. H. Muller, in Advances in Electrochemistry and Electrochemical Engineering, Vol. 9, p. 167.
8. H. J. Mathieu, LBL-1470 (1973).
9. H. J. Mathieu, LBL-2517 (1973).
10. The flow channel had a length of 90 cm with an entrance length of 76 cm. The hydraulic diameter is 1.3 cm. Flow velocity could be varied by means of a manual valve. A 20ℓ tank was positioned 1.7m above the top of the channel to give flow velocities up to 140 cm/s.
11. W. Pourbaix, Atlas of Electrochemical Equilibria in Aqueous Solutions (Pergamon Press, 1966), p. 384.
12. A refractive index n = 1.352-0.0001i was assumed for the boundary layer. Experiments with other copper salt solutions[16] show a change of the real part of the refractive index of $\Delta n = 0.029c$. The

concentration of the boundary-layer solution was assumed to be $c = 6 \times 10^{-2}$ mol/ℓ. It could not be determined definitely whether the boundary layer consisted of $CuClO_3$ or $Cu(ClO_3)_2$ or both, because both solutions would give only a small change in optical constants. A small absorption coefficient k = 0.0001 has to be assumed for the boundary layer.[17,18]

13. Porosity derived by linear interpolation of refractive indices.

14. F. W. Young, Diss. University of Virgina, 1950.

15. P. C. Lodelfe, A. W. Czandemo and J. R. Biegen, Thin Sol. Films 10, 403 (1972).

16. F. R. McLarnon, R. H. Muller and C. W. Tobias, LBL-2240 (in preparation).

17. Gmelin, Handbuch 60, B1, 333 (1958).

18. E. Müller, Ann. Phys. 12, 767 (1903).

19. H. Schopper, in Landolt-Bornstein, Vol. II, part 8, (Springer, Berlin, 1962), p. 1.

20. L. G. Schulz, J. Opt. Soc. Am. 44, 357 (1954); L. G. Schulz and F. R. Tangherlini, J. Opt. Soc. Am. 44, 362 (1954).

21. J. V. Cathcart, G. F. Petersen, Ellipsometry in the Measurement of Surfaces and Thin Films, NBS Misc. Publ. 256 (1963), p. 201.

22. Mixture of resins 70% Shell 826, 17.5% Dow Corning 736 and 12.5% Ciba D40; oven-cured.

FIGURE CAPTIONS

Fig. 1. Block diagram of self-nulling ellipsometer.

A	analyzer
AF	analyzer Faraday cell
C	collimator
CT	controller
DVM1	digital voltmeter indicating polarizer rotation
DVM2	digital voltmeter indicating analyzer rotation
F	filter (λ = 546.1 nm)
G1	galvanometer-oscillograph for polarizer rotation
G2	galvanometer-oscillograph for analyzer rotation
L	high pressure mercury arc lamp
M1	polarizer AC-power supply
M2	analyzer AC power supply
O	oscillator
P	polarizer
PF	polarizer Faraday cell
PM	photomultiplier
PS1	polarizer DC power supply
PS2	analyzer DC power supply
Q	compensator
S	sample
T	telescope

Fig. 2. Cross section of open, stagnant solution cell.

A cell body

B observed electrode (anode), 1.2×3 cm area

C body for observed electrode (cast epoxy, exchangeable)

D electrical connection for observed electrode (brass, silver-soldered to electrode)

E sealing nut for electrode body (polypropylene)

F washer (Teflon)

G O-ring for electrode body (Silicone rubber)

H holder for electrode body (polypropylene)

I screws to attach observed electrode with holder to stagnant cell

J O-ring seal for electrode holder

K frame for window (acrylic, clued to cell body)

L sealing nut for window (acrylic)

M frame for diaphragm

N diaphragm (polyester cloth)

O counter-electrode (stainless, 0.018 in.×2 1/8 in.×2 1/2 in.)

P O-ring for cell window

Q cell window

R pressure sleeve for cell window (acrylic)

Fig. 3. Cross-section of flow channel cell.

A body of flow channel (acrylic resin)

B observed electrode (anode), 1.2×3 cm area

C body for observed electrode (cast epoxy,[22] exchangeable)

D electrical connection for observed electrode (brass, silver-soldered to electrode)

E sealing nut for electrode body (polypropylene)

F washer (Teflon)

G O-ring for electrode body (silicone rubber)

H holder for electrode body (polypropylene)

I screws to attach observed electrode with holder to flow channel

J O-ring seal for electrode holder

K counter electrode (cathode), 0.9×2.5 cm area (314 stainless)

L sealing material for rectangular counter electrode in round cavity (epoxy resin)

M stem for counter-electrode (stainless, silver-soldered)

N O-ring seal for counter electrode

O acorn nut with electrical connection for counter electrode (stainless)

P electrical connection for counter-electrode

Q cell window (plate glass, 0.25 in. thick, 0.7 in. diam.)

R O-ring for cell window

S pressure sleeve for cell window (PVC)

T sealing nut for cell window (brass)

Fig. 4. Typical recorder trace of ψ and Δ vs t for 125 mA/cm^2 in stagnant solution (free convection). Dashed lines are computed values of ψ and Δ for a compact layer of Cu_2O (n = 2.75-0.25i) for thickness 0-2500Å and a porous layer (n = 2.05-0.25i) for 2500-6000Å.

Fig. 5. Preliminary interpretation of ellipsometer measurements (solid line) of the anodic dissolution of Cu in stagnant 2M $NaClO_3$ at 112 mA/cm^2. Calculations (dashed line) based on the optical constants of a compact oxide layer. n_o = 1.35, n_{Cu} = 0.93-2.39i n_{Cu_2O} = 2.75-0.25i (2.75-0.2i for triangles).

Fig. 6. Effect of increased current density on ψ vs t curve for (a) 112 mA/cm^2, (b) 270 mA/cm^2, (c) 430 mA/cm^2.

Fig. 7. ψ vs Δ plot of four experiments obtained at 125 mA/cm^2 and different flow velocities. (a) u = 0 cm/s, (b) u = 5.93 cm/s. (c) u = 14.6 cm/s and (d) u = 44.8 cm/s.

Fig. 8. Film growth of a Cu_2O oxide film in stagnant 2M $NaClO_3$ solution without any current.

Fig. 9. (a) Two-layer model for film, (b) step 1, (c) step 2 of computation.

Fig. 10. Effect of Cu_2O layer thickness and imaginary part of boundary layer refractive index on expected ψ and Δ. (a) Measured data, (b) computed for n = 1.352-0.0001i, no Cu_2O, (c) n = 1.352-0.0002i, no Cu_2O and (d) computed for n = 1.352-0.0001i, 20Å Cu_2O, n_{Cu_2O} = 2.75-0.25i.

Fig. 11. Effect of variation of optical constants of oxide film in the presence of a mass transfer boundary layer (computed).

a) $n_{Cu_2O} = 2.75-0.25i$

b) $n = 2.05-0.25i$

c) $n = 1.8-0.25i$

d) $n = 0.6-0.25i$

e) $n = 1.4-0.25i$

f) $n_{CuO} = 2.56-0.539i$

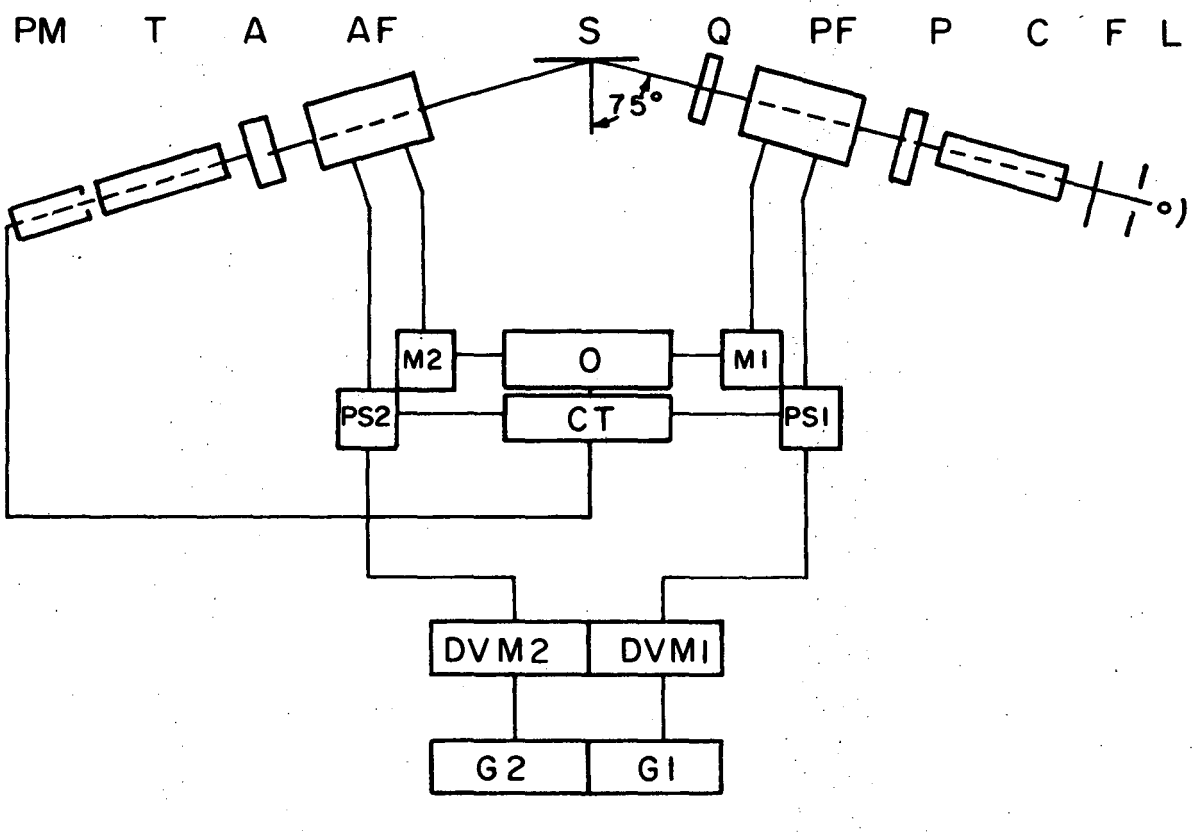
PM
T
A
AF
S
Q
PF
P
C
F
L
75°
M2
O
M1
PS2
CT
PS1
DVM2
DVM1
G2
G1
XBL7310 - 4210

Fig. 1

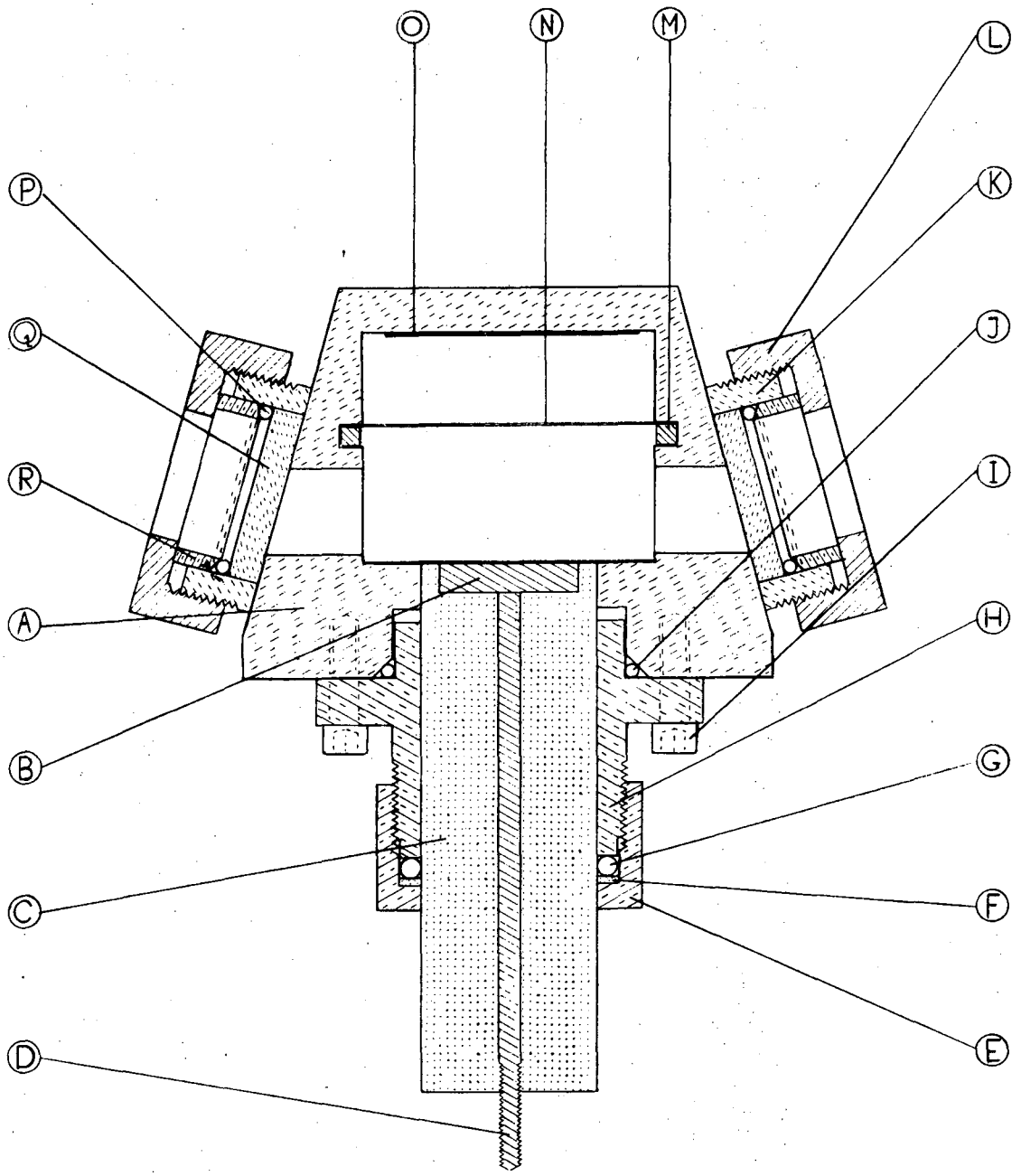

Fig. 2

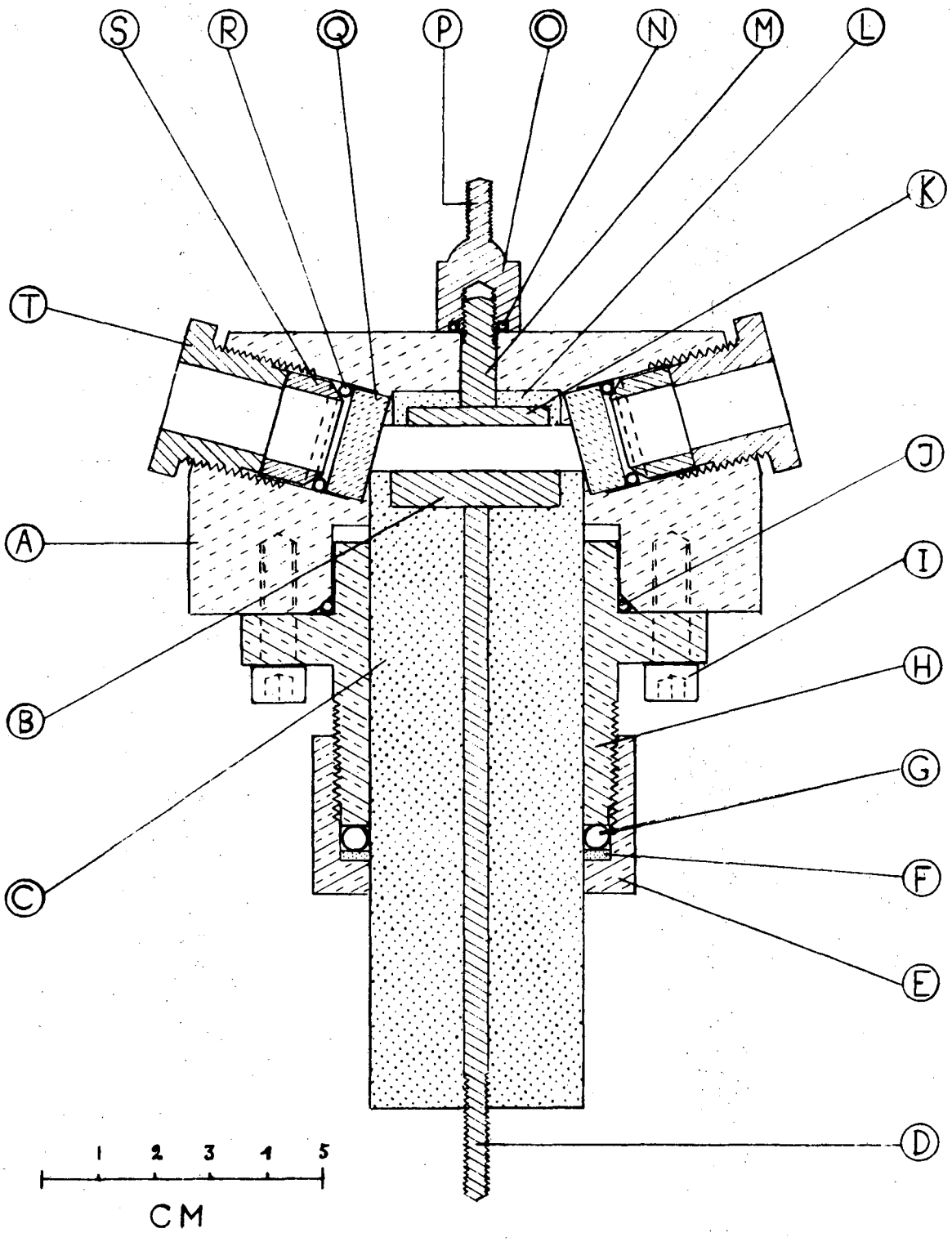

XBL 741-34

Fig. 3

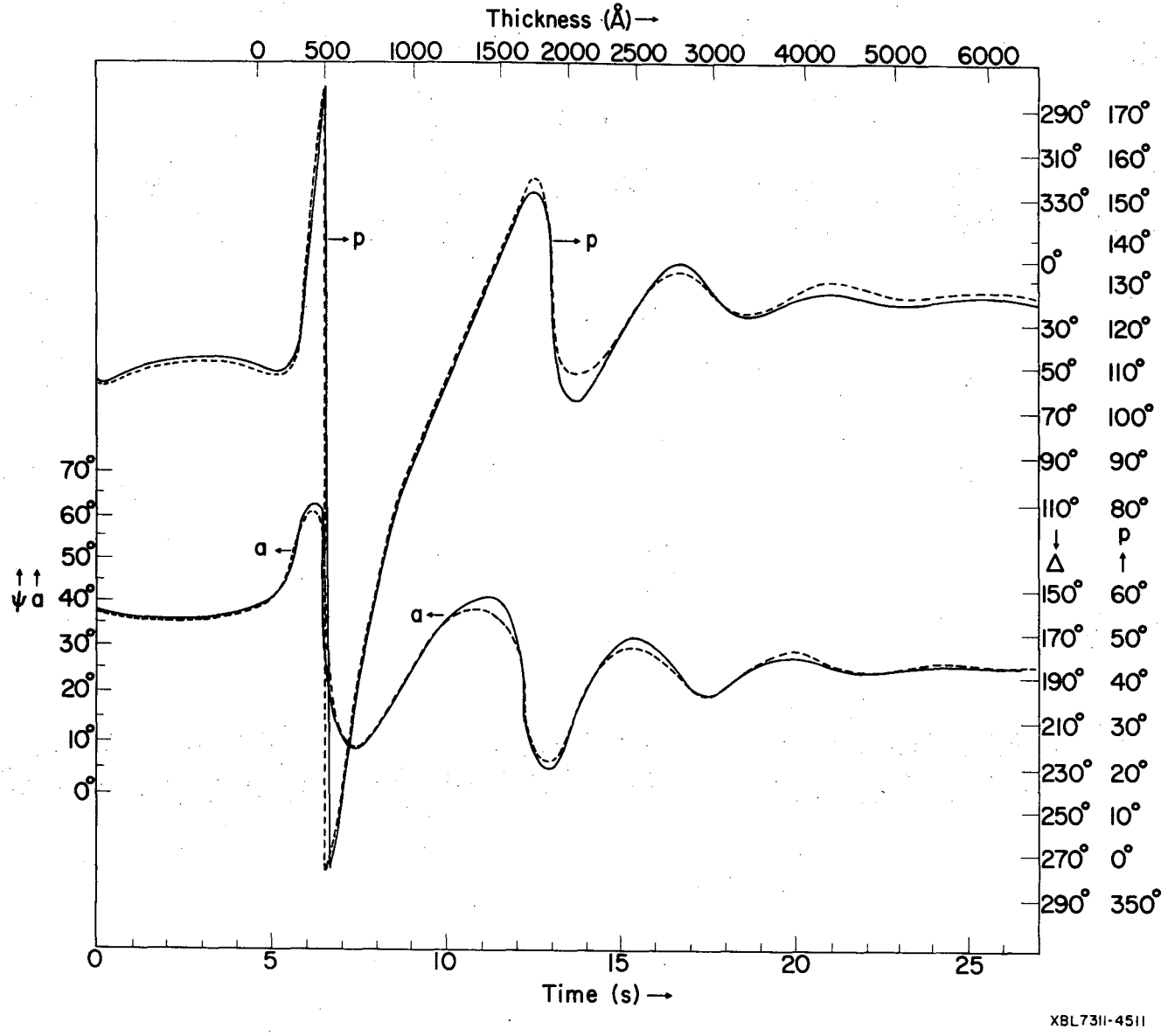
Thickness (Å)→
0 500 1000 1500 2000 2500 3000 4000 5000 6000
p
p
a
a
70° 60° 50° 40° 30° 20° 10° 0°
ψa
290° 310° 330° 0° 30° 50° 70° 90° 110°
170° 160° 150° 140° 130° 120° 110° 100° 90° 80°
Δ
p
150° 170° 190° 210° 230° 250° 270° 290°
60° 50° 40° 30° 20° 10° 0° 350°
0 5 10 15 20 25
Time (s)→
XBL7311-4511

Fig. 4

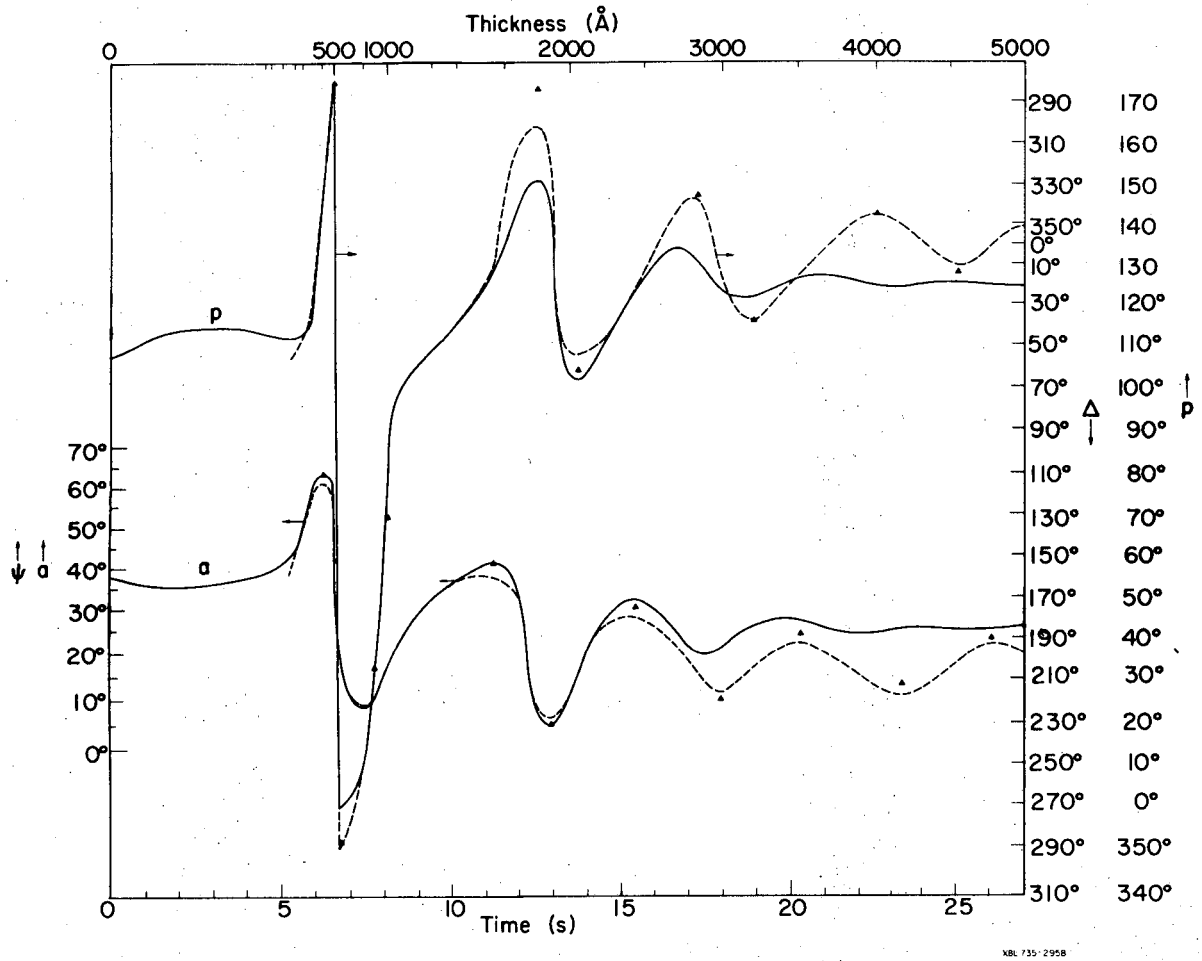
Thickness (Å)
0
500 1000
2000
3000
4000
5000
p
a
70°
60°
50°
40°
30°
20°
10°
0°
Ψ a
290 170
310 160
330° 150
350° 140
0° 130
10° 120°
30° 110°
50° 100°
70° 90°
90° 80°
110° 70°
130° 60°
150° 50°
170° 40°
190° 30°
210° 20°
230° 10°
250° 0°
270° 350°
290° 340°
310°
Δ
p
0
5
10
15
20
25
Time (s)
XBL 735-2958

Fig. 5

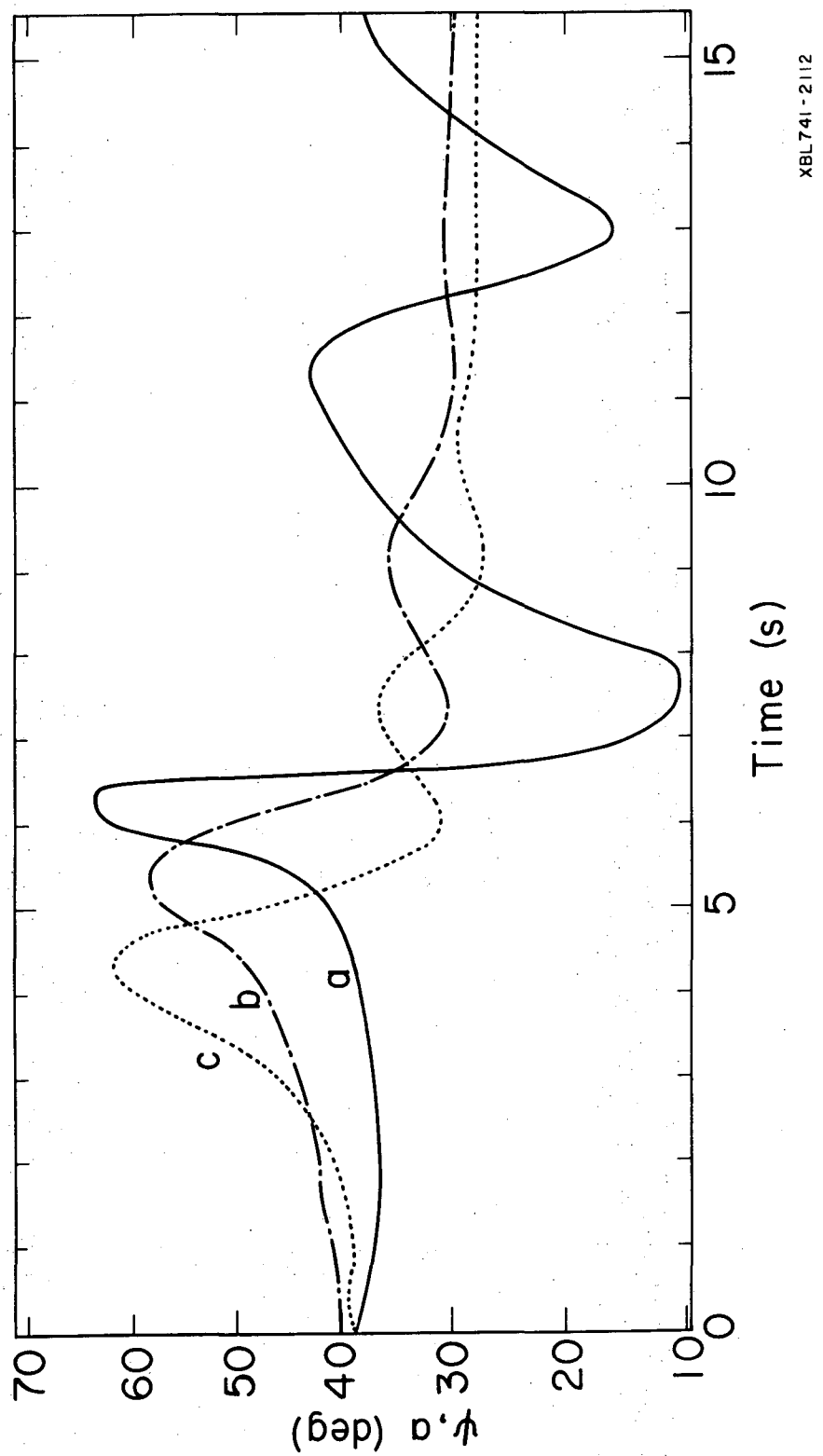

Fig. 6

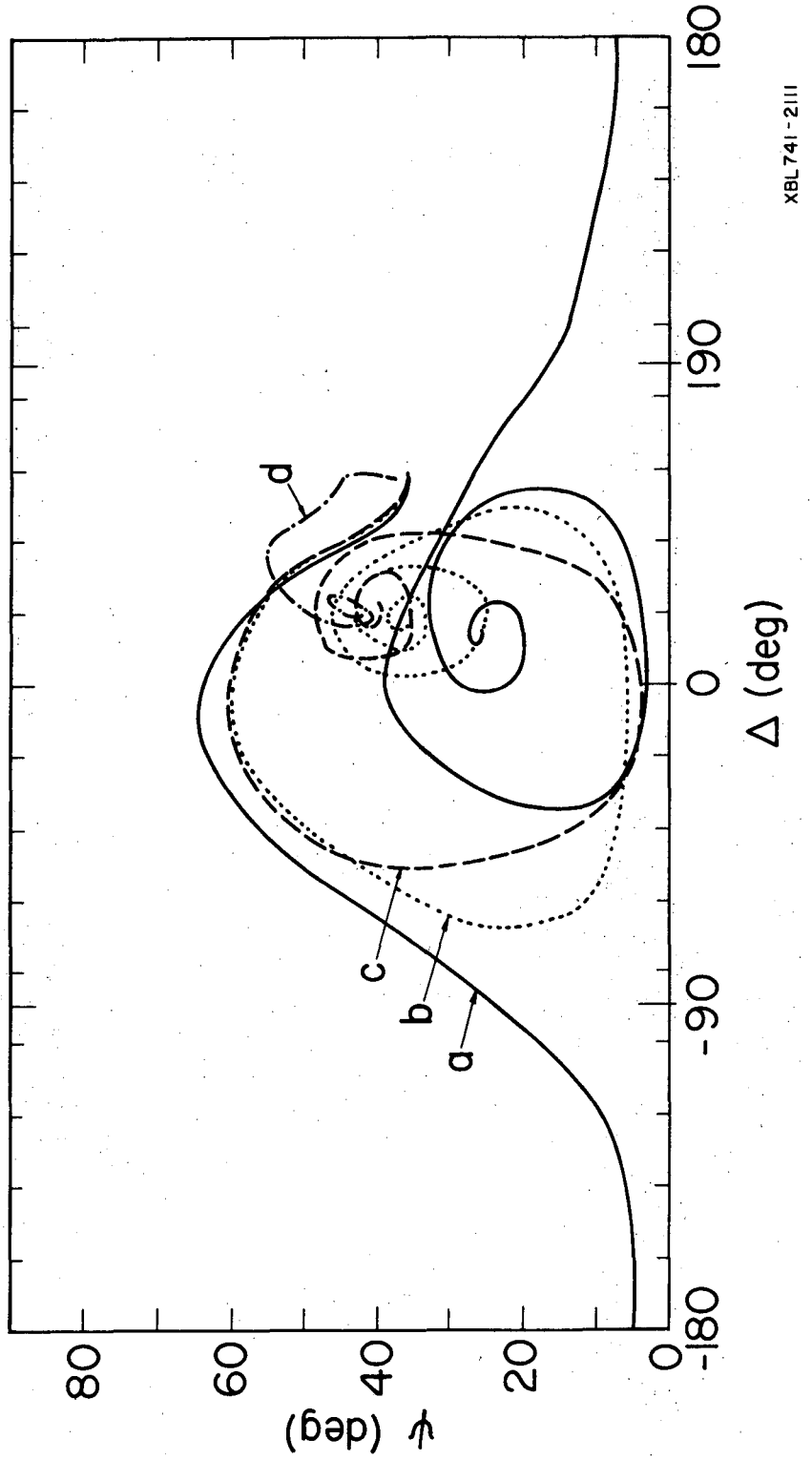

Fig. 7

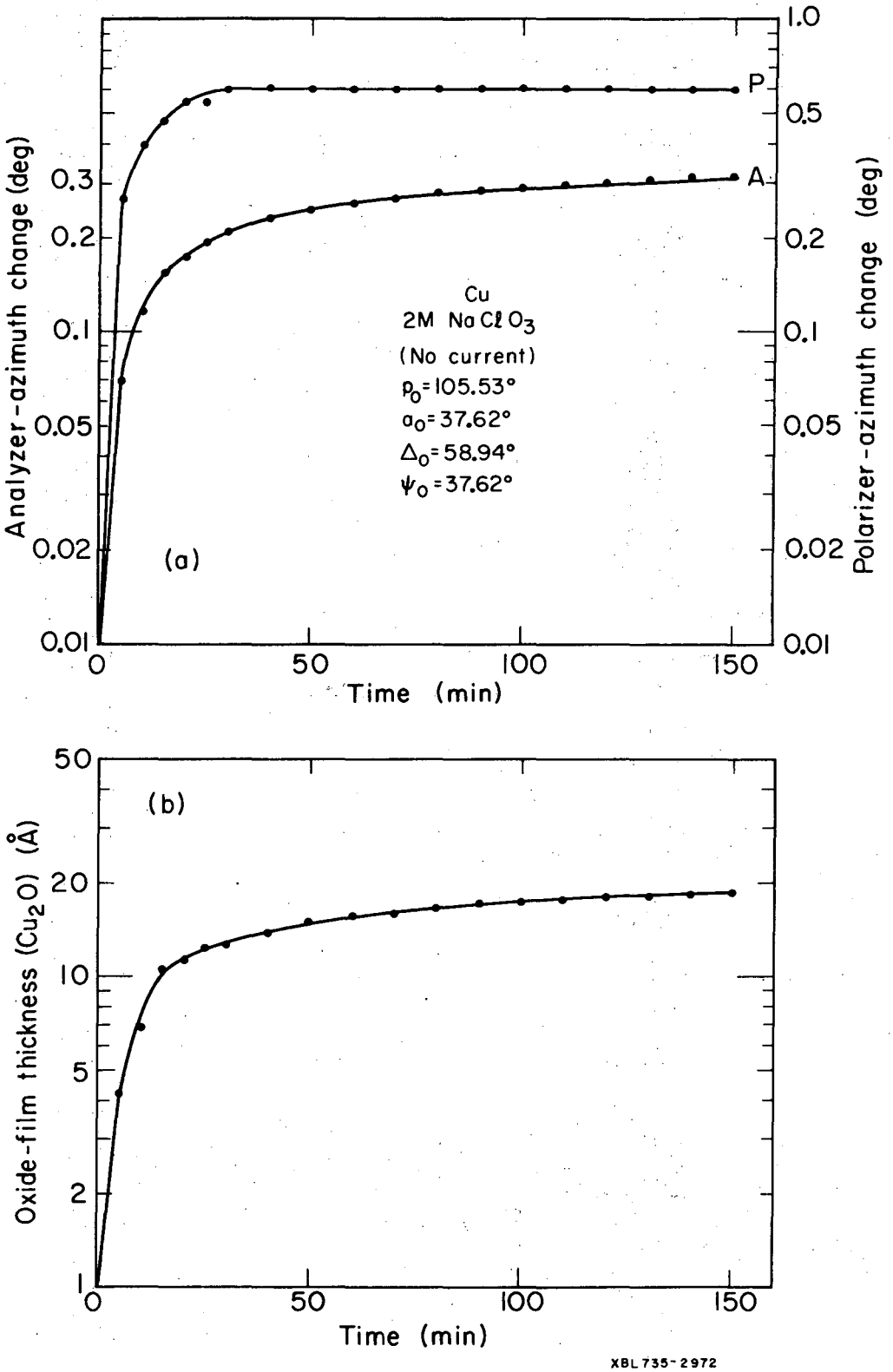
Analyzer-azimuth change (deg)
Polarizer-azimuth change (deg)
Time (min)
P
A
Cu
2M NaClO3
(No current)
p0=105.53°
a0=37.62°
Δ0=58.94°
ψ0=37.62°
(a)
(b)
Oxide-film thickness (Cu2O) (Å)
XBL735-2972

Fig. 8

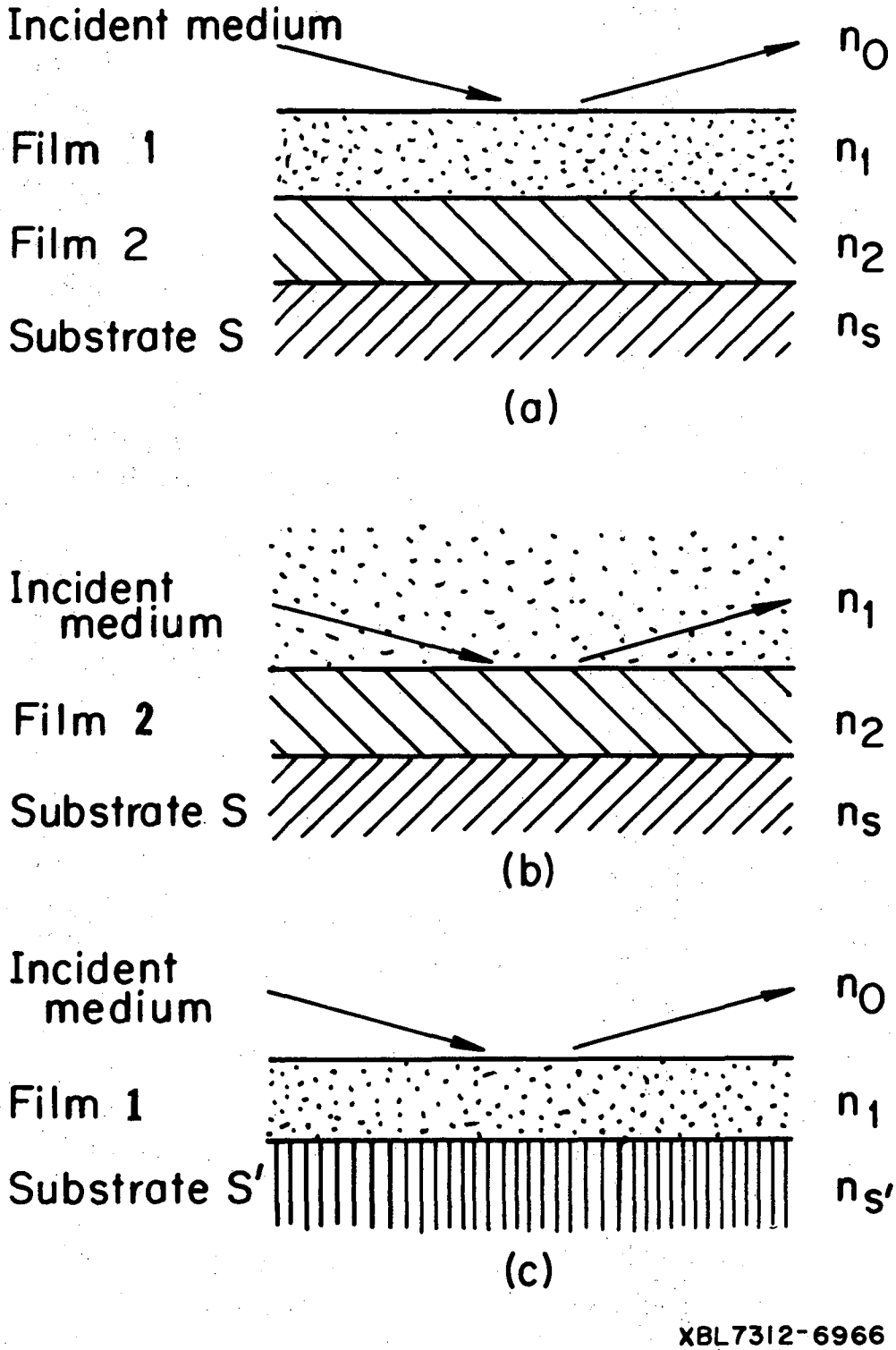
Incident medium
n_0
Film 1
n_1
Film 2
n_2
Substrate S
n_s
(a)
Incident medium
n_1
Film 2
n_2
Substrate S
n_s
(b)
Incident medium
n_0
Film 1
n_1
Substrate S'
$n_{s'}$
(c)
XBL7312-6966

Fig. 9

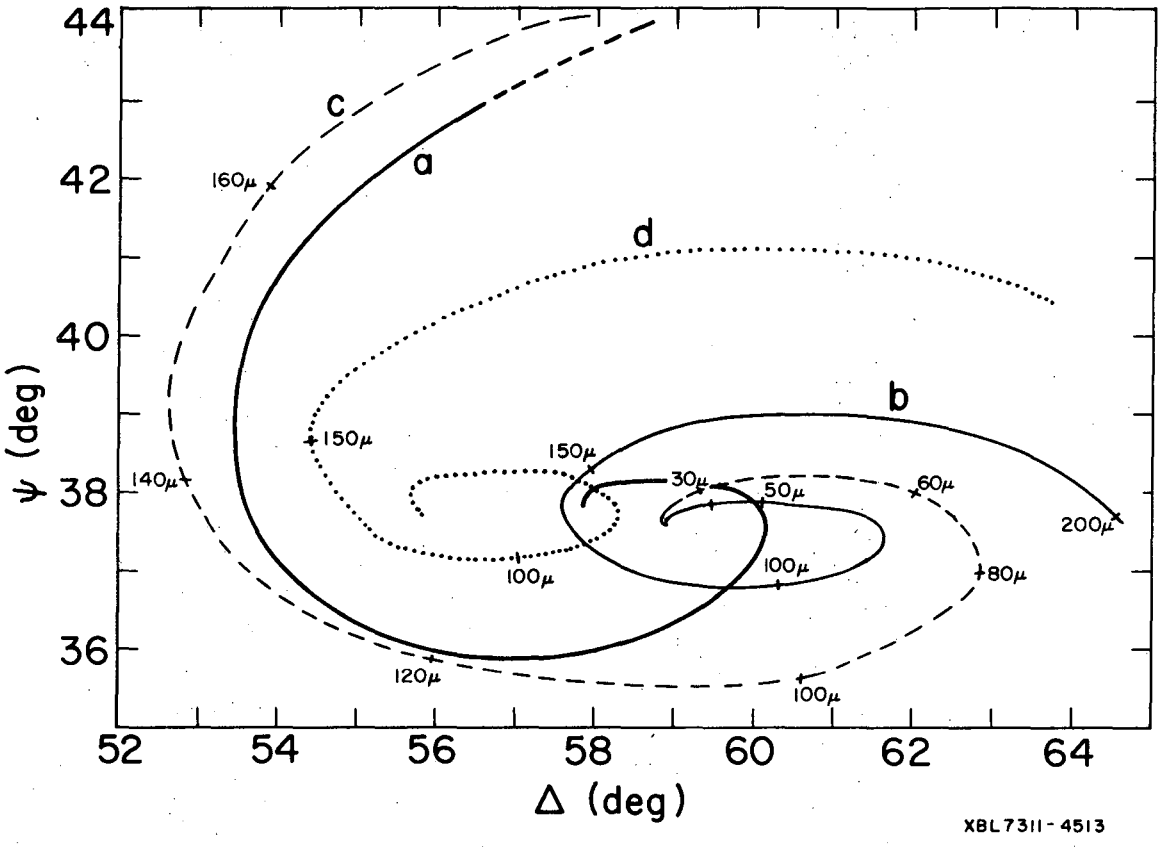
44
42
40
38
36
ψ (deg)
52
54
56
58
60
62
64
Δ (deg)
a
b
c
d
160μ
140μ
150μ
150μ
30μ
50μ
60μ
200μ
100μ
100μ
80μ
120μ
100μ
XBL7311-4513

Fig. 10

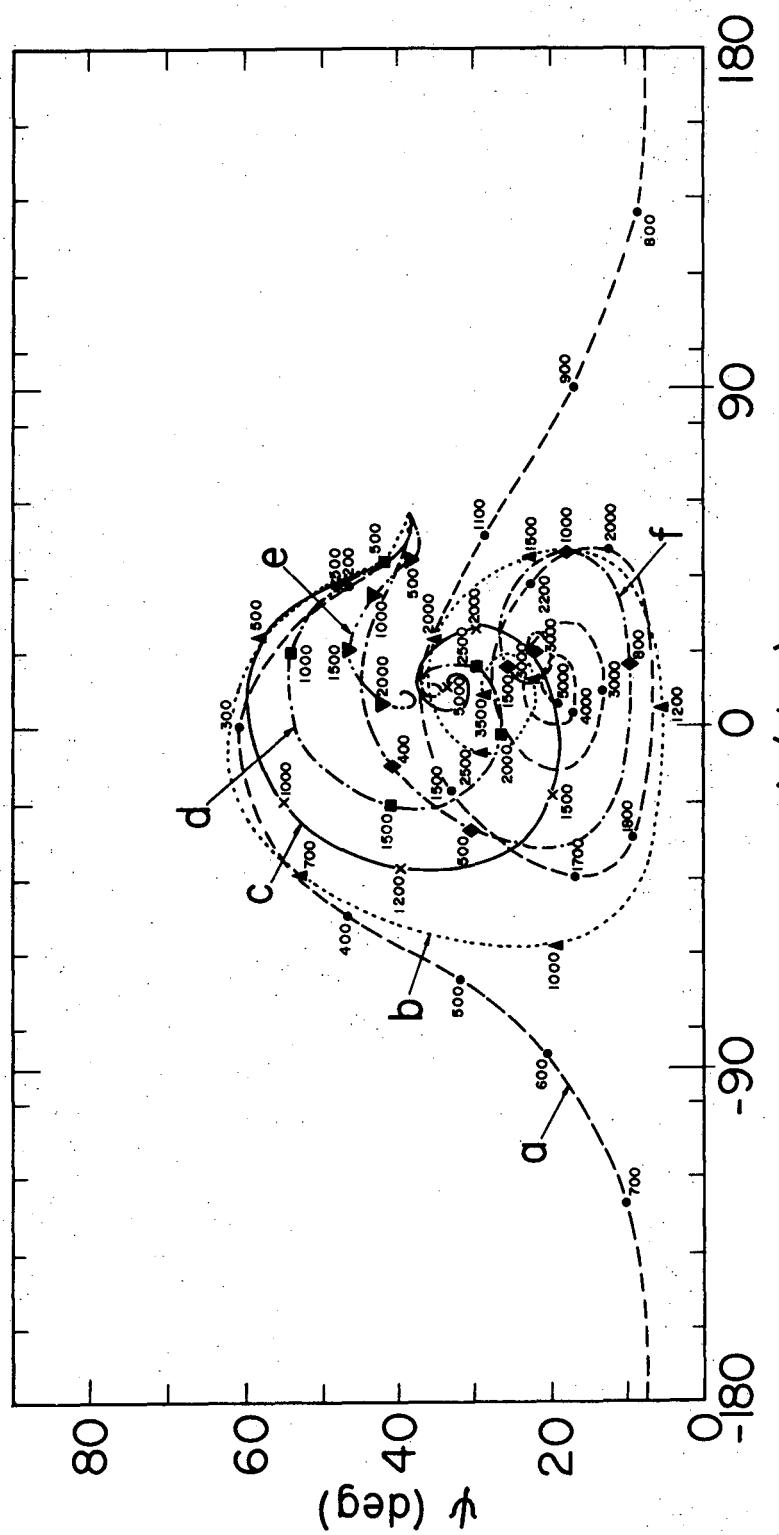

XBL741-2149

Fig. 11

TECHNICAL INFORMATION DIVISION
LAWRENCE BERKELEY LABORATORY
UNIVERSITY OF CALIFORNIA
BERKELEY, CALIFORNIA 94720